The combined influence of the stratospheric polar vortex and ENSO on zonal asymmetries in the Southern Hemisphere upper tropospheric circulation during austral spring and summer

To link to this article DOI: http://dx.doi.org/10.1007/s00382-022-06225-0

Publisher: Springer

Noname manuscript No.
(will be inserted by the editor)

The Combined Influence of the Stratospheric Polar Vortex and ENSO on Zonal Asymmetries in the Southern Hemisphere Upper Tropospheric Circulation during Austral Spring and Summer

Marisol Osman · Theodore G. Shepherd · Carolina S. Vera

Received: date / Accepted: date

Abstract The influence of El Niño Southern Oscillation (ENSO) and the Stratospheric Polar Vortex (SPV) on the zonal asymmetries in the Southern Hemisphere atmospheric circulation during spring and summer is examined. The main objective of the work is to explore if the SPV can modulate the ENSO teleconnections in the extratropics. We use a large ensemble of seasonal hindcasts from the European Centre for Medium-Range Weather Forecasts Integrated Forecast System to provide a much larger sample size than is possible from the observations alone. We find a small but statistically significant relationship between ENSO and the SPV, with El Niño events occurring with weak SPV and La Niña events occurring with strong SPV more often than expected by chance, in agreement with previous works. We show that the zonally asymmetric response to ENSO and SPV can be mainly explained by a linear combination of the response to both forcings, and that they can combine constructively or destructively. However the nature of this interference evolves through the spring and summer period, and is not aligned with the traditional seasons. From this perspective, we find that the tropospheric asymmetries in response to ENSO are more intense when El Niño events occur with weak SPV and La Niña events occur with strong SPV, at least from September through December. In the stratosphere, the ENSO teleconnections are mostly confounded by the SPV signal. The analysis of Rossby Wave Source and of wave activity shows that both are stronger when El Niño events occur together with weak SPV, and when La Niña events occur together with strong SPV.

Keywords Rossby Waves · Teleconnections · Wave-Activity Fluxes

M. Osman
Departamento de Ciencias de la Atmósfera y los Océanos, Facultad de Ciencias Exactas y Naturales, Universidad de Buenos Aires. Centro de Investigaciones del Mar y la Atmósfera (CIMA), Instituto Franco-Argentino del Clima y sus Impactos (UMI-IFAECI) /CNRS, CONICET, Universidad de Buenos Aires, Buenos Aires, Argentina.
E-mail: osman@cima.fcen.uba.ar

1 Introduction

The variability of the high-latitude Southern Hemisphere (SH) springtime and summertime atmospheric circulation is dominated by the Southern Annular Mode (SAM) and by teleconnections emanating from tropical latitudes. These teleconnections emerge as a response to changes in tropical convection such as those arising during El Niño-Southern Oscillation (ENSO) (Mo, 2000). Many works have described the influence of ENSO on the high latitudes through changes in the eddy-driven zonal circulation (Seager et al., 2003; L'Heureux and Thompson, 2006) and in the zonally asymmetric circulation (Kidson, 1999; Mo, 2000; Vera et al., 2004; Ding et al., 2012; Wilson et al., 2016). In the case of the zonally asymmetric circulation, these changes occur mainly through the modulation of the Pacific South America (PSA) pattern, an alternating wave-train of pressure anomalies emanating from the tropics in response to convection in the Tropical Pacific. In addition, some works have assessed how the SAM modulates the variability of ENSO teleconnections, especially over the South Pacific (Silvestri and Vera, 2003; Fogt and Bromwich, 2006; Fogt et al., 2011). In particular, Fogt et al. (2011) found that the SAM phase and magnitude modulate the South Pacific ENSO teleconnection through an interaction between the ENSO-induced and SAM-induced anomalous eddy momentum fluxes.

Another feature of the SH high-latitude circulation during spring to early summer is that the stratosphere-troposphere coupling peaks, associated with variability in the timing of the SH Stratospheric Polar Vortex (SPV) breakdown (Thompson and Wallace, 2000). During this period, the zonal-mean extratropical circulation is organized under the influence of the SPV (Black and McDaniel, 2007), with a tendency of early breakdown events to be associated with a more equatorward tropospheric jet transition, and of late breakdown events to be associated with a delay in this transition (Byrne et al., 2017). The variability in the tropospheric circulation that follows the anomalies in the SH stratospheric zonal flow can persist for up to three months (Thompson et al., 2005). The variability of the SPV is also related to the phase of ENSO, with a tendency of having early vortex breakdown events during El Niño years and late vortex breakdown events during La Niña years (Byrne et al., 2017). These results support the idea that, while it was previously believed that the eddy-driven jet responds directly to the tropical forcing associated with ENSO (L'Heureux and Thompson, 2006), the zonally symmetric component of the response appears to be primarily through the stratosphere (Byrne et al., 2019). ENSO can also modify the planetary stratospheric waves in spring and summer and affect the phase of the quasi-stationary waves (Hurwitz et al., 2011; Lin et al., 2012; Zubiaurre and Calvo, 2012). This relationship between ENSO, the eddy-driven jet and the SPV, combined with the previous findings on the SAM modulation of ENSO teleconnections in the South Pacific, suggest the idea of an SPV influence on zonal asymmetries in the SH in response to ENSO, at least during spring and summer. This stratospheric modulation of the asymmetric circulation has been widely documented for the Northern Hemisphere (Ineson and Scaife, 2009; Butler et al., 2014) but in the SH has received less attention.

While these studies have advanced the understanding of the ENSO-SPV relationship, many of them are based on reanalyses or observations, which limits the confidence in the results due to the uncertainty associated with the limited sample size. The non-random joint distribution of ENSO and SPV anomalies complicates the analysis of the climate response to both forcings because regressing on one index alone could introduce a confounding influence of the other index. Regressing out one variable is the usual way to treat this limitation, but it assumes linearity in the relationship and also requires a long observational record. Byrne et al. (2019) addressed both issues (sample uncertainty and linearity of the relationship) by using a large ensemble of data to study the zonally symmetric response to ENSO and SPV. In this work we propose a similar approach to investigate the asymmetric response to both forcings.

The objective of this paper is then to study the combined influence of ENSO and the SPV on the zonal asymmetries of the atmospheric circulation in the SH. We use a large ensemble of seasonal hindcasts from ECMWF System 4 to address the impact of sampling uncertainty and to allow for the detection of nonlinearities in the response to each forcing. The large sample size also allows for detection of signals on a subseasonal (monthly) timescale. We begin by describing the model and methodology used in the study. The results section encompasses the assessment of the model in simulating anomalies in the SH and the study of the joint influence of SPV and ENSO on the tropospheric anomalies. Finally we discuss the generation and propagation of Rossby waves, followed by the conclusions.

2 Data and Methods

The European Centre for Medium-Range Weather Forecasts System 4 hindcasts were used in the study. The System 4 hindcast ensemble has proven to represent a more realistic circulation variability at polar latitudes than the ECMWF System 5 hindcast (Shepherd et al., 2018), possibly due to a better representation of stratospheric variability in the SH. System 4 (S4) consists of the Integrated Forecasting System (IFS) atmospheric component coupled to the Nucleus for European Modelling of the Ocean (NEMO) ocean model (Molteni et al., 2011). The atmospheric vertical resolution is 91 levels, with a top model level in the mesosphere at 0.01hPa, and the horizontal spectral resolution is T255, which corresponds to approximately 80 km in the horizontal. The resolution of the ocean model is 1° in the horizontal and has 42 layers in the vertical. All hindcasts are issued as ensembles with 51 members. Here we consider hindcasts initialized on 1 August over the period 1981-2018 for austral spring and summer (September-February). We excluded 2002, the year of the Stratospheric Sudden Warming in the SH, from our analysis so that our results are not influenced by this anomalous event. However, we have checked that our results are not significantly affected by this procedure. The variables used in the study are geopotential height, zonal and meridional winds from 200hPa and 50hPa to characterize the upper troposphere and the stratosphere, respectively. The ERA-Interim reanalysis was used as observations (Dee et al., 2011).

Following Byrne et al. (2019) (see also Hio and Yoden, 2005; Kuroda and Kodera, 1998) we define an index of interannual stratospheric variability as the leading principal component time series resulting from the empirical orthogonal function (EOF) analysis on monthly mean geopotential height at 50hPa averaged over the polar cap (60°S-90°S). The method consists of combining X successive months of data in a vector for a given year and therefore each eigenvector has X elements. In this study, X is set to 7 to span the August-February period. We define weak stratospheric polar vortex (SPV) years as those years in the upper quartile of the index (i.e. highest geopotential height) and strong SPV years as those in the lower quartile (i.e. lowest geopotential height). Likewise, we define an ENSO index as the leading principal component time series associated with the EOF analysis of monthly mean sea-surface temperature averaged over the Niño 3.4 region (5°N-5°S: 170°W-120°W). El Niño years are defined as those in the upper quartile of this index and La Niña years as those in the lower quartile.

3 Results

3.1 Model Assessment

We start with the validation of the model by comparing the upper tropospheric circulation during austral spring and summer in the S4 hindcast ensemble against the ERA-Interim reanalysis. Figures 1 and 2 show the mean differences in geopotential height and zonal wind at 200hPa, respectively, between hindcast and reanalysis from September until February. In the supplementary material we include the same figures for 50hPa. Overall, the model underestimates the geopotential height and the bias maximum shifts and increases from polar latitudes in September, October, November to low latitudes from December onward. The zonal wind bias is positive at tropical latitudes and negative at extratropical latitudes, peaking where the Subtropical Jet and the Eddy Driven Jet are manifest. The differences between the ERA-Interim and hindcast variances (see supplementary material Figures S1 and S2) are significant in small regions. Finally, the model bias in the mean and variance in geopotential height at 50hPa (see supplementary material Figures S3 and S4) resembles that documented for 200hPa while the bias in zonal wind at 50hPa is significant mainly at midlatitudes (see supplementary material Figures S5 and S6).

Next, we compare the model and ERA-Interim anomalies in response to ENSO and the SPV. As an example, Figure 3 shows composites of zonal asymmetries of the geopotential height (Z^*, anomalies with respect to the zonal mean field) at 200hPa for El Niño minus La Niña in October for the model and for ERA-Interim. Similar results are obtained for the other months considered in the study. The Pacific-South American pattern is present in both composites, although model anomalies look elongated in the zonal direction and negative anomalies are weaker in the model. The composites for weak minus strong SPV events (Figure 4) for the same month and level are also well represented by the model at polar latitudes although anomalies in the model span a larger portion over Antarctica than the observed counterpart. At midlatitudes larger differences are observed in the eastern Pacific and South America. At 50hPa the model reproduces better the composites for SPV events than for ENSO events (see supplementary material Figures S7 and S8). For the latter, the largest differences are observed over the Indian Ocean and high latitudes, where negative anomalies in the model are weaker and span a smaller area than in the reanalysis.

Overall, despite the mean biases there appears to be good agreement between the hindcasts and the ERA-Interim reanalysis in the representation of the anomalies in response to ENSO and the SPV in the troposphere as well as in the stratosphere. On that basis we proceed to examine their interdependences, exploiting the large sample size provided by the hindcast ensemble.

3.2 ENSO-SPV relationship in the hindcast ensemble

Figure 5 shows the joint distribution of the ENSO and SPV indices for the hindcast realizations and Table 1 lists the number of realizations falling in each category. We performed a chi-square test on the 3 x 3 contingency table of the joint ENSO-SPV distribution to determine if the distribution is different from the expected contingency table drawn from independent variables. Nine categories are defined according to whether SPV and/or ENSO indices lie in the lower or upper quartile or are neutral. The correlation between SPV and ENSO indices is low (0.18), in agreement with previous works (Silvestri and Vera, 2009; Fogt et al., 2011), but is nevertheless statistically significant given the large number of cases considered. From the table it is clear that the Niño-strong SPV and Niña-weak SPV combinations are more underpopulated than expected by chance, and the chi-square test suggests that the null hypothesis of independent categories does not stand (p-value of 9e-11, much smaller than 0.01). This uneven distribution of joint ENSO-SPV events is also observed when deciles instead of quartiles are used to determine cases (p-value of 5e-7). Fogt et al. (2011) found a similar result when the observed ENSO-SAM relationship during the 1957-2009 period was considered, with a prevalence of El Niño occurrence during negative SAM and of La Niña occurrence during positive SAM, primarily during the December-January-February season. If we associate positive SAM with strong SPV (and late vortex breakdown) and negative SAM with weak SPV (and early vortex breakdown), then Figure 5 and Table 1 are in agreement with the hypothesis of Byrne et al. (2017) of a stratospheric pathway for the ENSO-SAM relationship. Following previous works, in the remaining text we will refer to in-phase events when both indices lie in the lower or upper quartile and are of the same sign, bearing in mind that strong SPV events are associated with a negative SPV index and weak SPV events with a positive SPV index, and to out-of-phase events when both indices are in the extreme quartiles but are of opposite sign.

3.3 Zonal asymmetries in response to ENSO and SPV events in the hindcast ensemble

We now analyze the joint influence of ENSO and the SPV on the circulation by investigating the zonal asymmetries in the stratosphere and troposphere. Because of the non-random joint distribution of ENSO and SPV anomalies, regressing on one index alone could introduce a confounding influence of the other index, complicating the physical interpretation. We can control for such a confounding influence by conditioning on the other variable. Thus, we first examine the influence of SPV conditional on either El Niño or La Niña conditions; and the influence on ENSO conditional on either a strong or weak SPV. This analysis also tests the linearity of the relationship, i.e. whether it is dependent on the state of the conditioning variable. We then examine all four corners of the contingency table, i.e. the two in-phase and two out-of-phase configurations of the ENSO and SPV indices. Table 2 summarizes the different composites computed. We do this for all the figures in this subsection.

Figures 6 and 8 show composites of Z^* at 50hPa and 200hPa, respectively, from September to February for weak minus strong SPV conditioned on El Niño events, weak minus strong SPV conditioned on La Niña events, El Niño minus La Niña conditioned on weak SPV events, and El Niño minus La Niña conditioned on strong SPV events. Figures 7 and 9 show composites of Z^* anomalies at 50hPa and 200hPa, respectively, for in-phase events and out-of-phase events. Coloured regions show statistically significant anomalies at the 5% level based on a t-test. In the stratosphere, the SPV composites conditioned either on El Niño or La Niña (Figure 6 two leftmost columns) present a wave-1 pattern with positive (negative) anomalies occupying most of the eastern (western) Hemisphere in September and October (first and second row). The asymmetries are very intense in middle and high latitudes. In November (third row), at polar latitudes the anomalies reduce their extension and in midlatitudes they shift westward. In December (fourth row), asymmetries are confined to high latitudes and are displaced 90° with respect to previous months. In January and February (fifth and sixth row) the anomalies are almost negligible. On the other hand, the ENSO composites conditioned either on weak or strong SPV (Figure 6 two rightmost columns) present more of a wave-2 pattern that is stronger and positive in the south Pacific Ocean and negative in the southeastern Indian Ocean and southwestern Atlantic Ocean in September and October. In November both positive and negative anomalies peak, with positive anomalies spanning the south Pacific Ocean as well as the southeastern Indian Ocean while negative anomalies are observed in the Atlantic Ocean. From December onward the anomalies are positive over the South Pacific and negative in the Atlantic and over Australia, although they are weaker than in previous months. At this level, the structure of the composites for joint ENSO-SPV events (Figure 7) retain the main characteristics of the SPV composites (that is, composites for strong/weak SPV together with El Niño or La Niña are similar to those for weak minus strong SPV conditioned on ENSO) in September and October, while in January and February the composites for joint ENSO-SPV events resemble those for El Niño minus La Niña conditioned on SPV. In November, the composites for in-phase events (Figure 7 two leftmost columns) are strong while in December the out-of-phase composites (Figure 7 two rightmost columns) are strong.

In the troposphere, the SPV composites conditioned on ENSO (Figure 8 two leftmost columns) present maximum asymmetries on both sides of the Antarctic peninsula peaking in October and decaying thereafter, being almost negligible in January and February. The ENSO composites conditioned on SPV (Figure 8 two rightmost columns) show the Pacific South American (PSA) pattern wave-train throughout the spring and summer time and peak in October and November. The composites for in-phase events (Figure 9 two leftmost columns) strengthen the PSA pattern observed in ENSO events, while the PSA is weaker when out-of-phase events are considered (Figure 9 two rightmost columns), in agreement with previous work (Fogt et al., 2011). It is noticeable that there is no signal at 200 hPa of the strong out-of-phase response observed at 50hPa in December.

We now assess whether the mentioned similarities and differences between composites for the different categories are statistically significant or not. To do this, we perform a statistical comparison of the composite fields by comparing the temporal-mean spatial fields (i.e. the composite anomalies) using the pattern correlation coefficient. We test the null hypothesis that the observed correlation is statistically indistinguishable from an unknown value between 0.9 and 1, which would result if both fields were drawn from the same population, instead of the usual test for correlation, which aims to determine if correlations differ significantly from zero. To evaluate the significance of this statistic we use a Monte Carlo method to avoid distortions due to the presence of spatial autocorrelation (Wigley and Santer, 1990). Following Wigley and Santer (1990) and Preisendorfer and Barnett (1983) we perform a Monte Carlo significance assessment through a Pool Permutation Procedure of 10000 permutations to obtain the p values. If two fields have a pattern correlation below 0.9 and a p value lower than 0.05 then the null hypothesis is rejected and the two spatial fields compared are considered to be statistically different. Since we are interested in determining the differences observed outside the tropics, correlations are only computed between gridpoints south of 45°.

Tables 3 and 4 show the pattern correlation between the composites of geopotential height for: weak minus strong SPV conditioned on El Niño against weak minus strong SPV conditioned on La Niña, El Niño minus La Niña conditioned on weak SPV against El Niño minus La Niña conditioned on strong SPV, the two in-phase events and the two out-of-phase events, for 50hPa and 200hPa, respectively. At both levels, the correlations are very high, at least during the spring. In the stratosphere, all the composites considered are not statistically different from unity, the only exception being for ENSO events conditioned on the SPV for January which is significant at the 10% level. Overall this supports the hypothesis of the linearity of the relationship. In the troposphere, the correlation between in-phase events and out-of-phase events is high and not statistically different from unity. However there is evidence of non-linearity in the other comparisons. During the September-December period, which is when the composites for SPV events conditioned on ENSO are meaningful, the correlation between those composites is statistically indistinguishable from unity only in September and October. Finally, the composites of El Niño minus La Niña conditioned on SPV events are highly correlated, but nevertheless those correlations are statistically different from unity during November, December and January.

Despite some evidence of non-linearity, the pattern correlations in Tables 3 and 4 are quite high except where the signals are weak. Thus overall, the ENSO response and the SPV response at high latitudes are mainly independent of the state of each other. Both responses can combine constructively or destructively, as is shown by the in-phase and out-of-phase composites, depending on the month considered. The correlations between composites conditioned on the different phases of each index also supports this hypothesis, at least during the spring.

4 Wave generation and propagation

Previous works investigated the mechanisms of how the tropical SST can influence the stratospheric circulation. Rossby wave theory suggests that changes in tropical convection can excite Rossby wave trains that propagate from the tropics into the extratropics, with some of them penetrating the stratosphere and changing the circulation there (Sardeshmukh and Hoskins, 1988). Lin et al. (2012) showed that Rossby wave trains emanating from the Pacific sector propagate southward and upward from their tropical source, with wave-train like patterns discernible in the troposphere as well as the stratosphere. The ENSO composites presented in the previous section show these wave train features in the troposphere and the stratosphere are in agreement with the ENSO composites shown by previous works (Lin et al., 2012; Hurwitz et al., 2011). Figure 10 shows composites of Rossby Wave Source (RWS) and divergent winds at 200hPa for the eight cases previously discussed against the climatology. Both variables are almost negligible, with the exception of a small region east of Australia, for composites of weak minus strong SPV conditioned on either El Niño or La Niña (first and second row). On the other hand, for El Niño minus La Niña events, conditioned on either weak or strong SPV (third and fourth row), RWS anomalies are negative over southeastern Australia and positive in the southeastern Pacific. Consequently, those regions also show significant convergent and divergent wind anomalies. When composites are computed for in-phase events (fifth and sixth row), RWS anomalies as well as divergent winds reinforce El Niño and La Niña signals to the east of Australia and span a larger area. This region of anomalous RWS lies in the core of the subtropical jet and could be responsible for the stronger Z^* anomalies emanating from the tropics and observed in the extratropical troposphere during in-phase events. Ding et al. (2012) showed that Rossby waves emanating from subtropical Australia propagate to west Antarctica, shaping the SAM pattern over the Amundsen Sea region. The strong anomalies observed on each side of the Antarctic Peninsula could be the result of the stronger RWS anomalies favoured by in-phase events. Conversely, the composites for El Niño and strong SPV (seventh row) (respectively La Niña and weak SPV, eighth row) present weaker RWS anomalies and weaker divergent winds than for El Niño and weak SPV (respectively La Niña and strong SPV), especially in the Pacific Ocean.

From the analysis presented we can infer that the effect of the different combination of drivers is mainly linear. The zonally asymmetric patterns are modulated in independent ways by ENSO and by SPV variability, although there is a correlation in the underlying variability, and these modulations can act either in-phase or out-of-phase. The position and intensity of the anomalies due to each forcing are the key to understand the composites observed for in-phase and out-of-phase events. We further explore the wave activity to understand the nature of the observed response. Figure 11 shows the ensemble mean horizontal wave-activity flux response and its divergence (Takaya and Nakamura, 2001) at 50hPa (left column) and 200hPa (right column) for the in-phase (first and second row) and out-of-phase events (third and fourth row). At 200hPa, the response spans the entire hemisphere and is stronger for in-phase events than for out-of-phase events, particularly in the South Pacific and Atlantic sectors. At 50hPa, wave activity fluxes are confined to middle and high latitudes and, as was observed for the troposphere, the response for in-phase events is stronger than for out-of-phase events, especially in the Pacific.

We decompose the ensemble-mean wave response into the ensemble-mean linear (EM_{LIN}) response and the ensemble-mean non-linear response (EM_{NL}, see appendix). This type of diagnosis has proven to be helpful in understanding the wave activity flux response to drivers (Fletcher and Kushner, 2011; Smith et al., 2010). The EM_{LIN} reflects the linear interference effect, that is, the phase difference between the wave response and the climatological wave. If wave responses are additive in the forcing, their EM_{LIN} terms should be additive. On the other hand, the EM_{NL} term reflects the effect associated with the wave response alone and is not additive. This analysis shows that EM_{LIN} is the dominant contributor to EM (see supplementary figures S9-S10). Therefore, most of the wave activity response is characterized by constructive or destructive interference between the ensemble mean response to both the SPV and ENSO driver and the climatological wave. The differences in the direction of the vectors between composites for strong/weak SPV and ENSO events can be related to the differences in the spatial coherence between the climatological wave-1 and -2 and the wave anomalies, which are of opposite sign between strong and weak SPV events and between El Niño and La Niña (not shown). For in-phase events the anomalous wave fluxes work together in the South Pacific and Atlantic sector while when out-of-phase events are considered the fluxes are weaker in the eastern South Pacific. The non-linear terms are smaller but still important. The EM_{NL} response for in-phase events shows highest activity and convergence and divergence in the southeastern Pacific sector, showing an eastward propagation, and in the Indian Ocean sector. This response is almost absent for out-of-phase events.

5 Conclusions

In this work we studied the combined influence of ENSO and the SPV on the zonal asymmetries in the extratropical SH during spring and summer. We used a large ensemble of seasonal forecast hindcasts to increase the robustness of the results and to avoid issues related to sampling uncertainty. The large sample size also allows an investigation of the subseasonal evolution of the ENSO and SPV influence through the spring/summer period, which is not well aligned with the traditional seasons (SON and DJF). Associating a strong SPV with a positive SAM and a weak SPV with a negative SAM, we found that the relationship between the ENSO and SAM observed in previous works also holds for ENSO and SPV with a tendency of El Niño (La Niña) events to be observed with weak (strong) SPV more often than expected by chance (Fogt et al., 2011; Fogt and Bromwich, 2006; Silvestri and Vera, 2003). In addition, the large sample size of the hindcast ensemble helps detect any non-linearities in the response to the ENSO and the SPV. We showed that the asymmetric response to ENSO and SPV can be mainly explained by a linear combination of the response to both forcings. In this sense, we found that the tropospheric asymmetries in response to ENSO are more intense when El Niño events occur with weak SPV and La Niña events occur with strong SPV (in-phase events), at least from September until December. In contrast, when out-of-phase events occur, the extratropical asymmetries observed are weaker than the typical ENSO response. This result extends the relationship between the ENSO teleconnection at midlatitudes with the phase of the tropospheric SAM found by Fogt et al. (2011) to the stratosphere, at least during the austral spring. In Figure 12 we present a schematic diagram that shows the influence of ENSO and SPV on the tropospheric zonal asymmetries and how both forcings combine during in-phase and out-of-phase events. ENSO composites conditioned on the strength of the SPV are independent of the status of the SPV (Figure 12a), while SPV composites conditioned on ENSO are independent of the phase of ENSO (Figure 12b). For in-phase events, the anomalies associated with SPV and ENSO reinforce each other mainly in the Pacific sector (Figure 12c), while the opposite happens during out-of-phase events (Figure 12d). In the stratosphere, the SPV signal dominates over the ENSO signal for September and October; while in November and December the asymmetries are stronger when in-phase and out-of-phase events are considered, respectively, implying that both drivers play a non-negligible role.

Note that the linearity of the asymmetric response to both forcings implies that the model biases documented in this study may not influence significantly the results presented, and helps explain why the model responses to forcings are quite realistic (Figures 3 and 4).

Previous works showed that Rossby wave trains emanating from the tropics associated with ENSO can propagate upwards to the stratosphere in midlatitudes (Hurwitz et al., 2011; Lin et al., 2012). We showed that tropospheric waves emanating from the tropical Pacific are stronger during in-phase events associated with a stronger RWS to the east of Australia. This can partially explain the stronger asymmetries observed during in-phase events. Our results are also in agreement with previous works that show that during in-phase events, enhanced eddy momentum fluxes are observed in the Pacific sector, which might be responsible for the stronger tropospheric asymmetries there (Fogt et al., 2011; Lin et al., 2012). Our interpretation is that both mechanisms can be argued to explain the observed response to ENSO and the SPV, and they are not incompatible (see Lin et al., 2012). This RWS analysis also suggests that the enhanced RWS observed during in-phase events could partially explain the correlation between the SPV and ENSO shown in Figure 5 and Table 1. More investigation is needed to assess this hypothesis, which is beyond the scope of the present study.

Having established the role of the SPV in shaping the extratropical asymmetric circulation response to ENSO, the question of the predictability associated with the occurrence of ENSO alongside with a strong/weak SPV arises. Previous works showed that predictability of the tropospheric circulation is larger during ENSO events than for non-ENSO events (Jha et al., 2016; Osman et al., 2016). In addition, the predictability of zonal circulation associated with SPV variability is larger during austral spring and summer (Seviour et al., 2014; Byrne et al., 2019). It could also be the case that the asymmetric circulation is more predictable when the ENSO manifests and the SPV varies from its climatological state. In a future work we will assess the predictability of the asymmetries reported in this work as well as the impact on surface variables, such as precipitation and temperature.

Acknowledgements Funding support is acknowledged from UBACyT20020170100428BA, PICT-2018-03046 and the CLIMAX Project funded by Belmont Forum/ANR-15-JCL/-0002-01, together with the European Research Council Advanced Grant 'Understanding the atmospheric circulation response to climate change' (ACRCC), project 339390. Support for an extended visit by M.O. to the University of Reading was also provided by the Department of Meteorology Visitors Programme. We acknowledge the provision of seasonal hindcast data from System 4 and the reanalysis data ERA-Interim by ECMWF. We would like to thank the two anonymous reviewers for their comments.

APPENDIX

A Wave activity flux decomposition

Wave activity fluxes are used to investigate the propagation of waves. We use the horizontal component of the wave activity flux $\boldsymbol{W}$ derived by Takaya and Nakamura (2001) which describes the propagation of wave disturbances on a zonally varying basic flow:

$$\boldsymbol{W} = \frac{1}{2\left|\overline{U}\right|} \begin{bmatrix} \overline{u}(\psi_x^{*2} - \psi^*\psi_{xx}^*) + \overline{v}(\psi_x^*\psi_y^* - \psi^*\psi_{xy}^*) \\ \overline{u}(\psi_x^*\psi_y^* - \psi^*\psi_{xy}^*) + \overline{v}(\psi_y^{*2} - \psi^*\psi_{yy}^*) \end{bmatrix}$$

where $\overline{U} = (\overline{u}, \overline{v})$ is the basic wind field and ψ^* is the streamfunction obtained from the zonal asymmetries Z^*. We decompose the ensemble mean of $\boldsymbol{W}$ (EM) into its linear term (EM_{LIN}) and non linear term (EM_{NL}). The decomposition follows Fletcher and Kushner (2011) and is illustrated here for the first term in the x-direction, but similar arguments apply to the rest of the terms. For each realization in the ensemble, we have

$$\psi^* = \langle \psi^* \rangle + {\psi^*}', \psi_x^* = \langle \psi_x^* \rangle + {\psi_x^*}', \psi_{xx}^* = \langle \psi_{xx}^* \rangle + {\psi_{xx}^*}'$$

where the angle brackets denote an ensemble mean and the prime a departure from the ensemble mean. The mean response, $\Delta \{...\}$, for the first term in the x-direction can be decomposed as

$$\Delta \left\{ \psi_x^{*2} - \psi^* \psi_{xx}^* \right\} = \Delta \left\{ \langle \psi_x^* \rangle^2 - \langle \psi^* \rangle \langle \psi_{xx}^* \rangle \right\} + \Delta \left\{ \left\langle {\psi_x^*}'^2 \right\rangle - \left\langle {\psi^*}' {\psi_{xx}^*}' \right\rangle \right\}.$$

The first term of the right-hand-side of the equation is the response associated with the ensemble mean eddy response (EM), while the second term is the response associated with the departures from the ensemble mean (FL). The EM term can be further decomposed if we separate the ensemble mean as follows:

$$\langle \psi^* \rangle = \psi_c^* + \Delta \langle \psi^* \rangle, \langle \psi_x^* \rangle = \psi_{xc}^* + \Delta \langle \psi_x^* \rangle, \langle \psi_{xx}^* \rangle = \psi_{xxc}^* + \Delta \langle \psi_{xx}^* \rangle$$

where the subscript c refers to the climatology. Then,

$$EM = EM_{LIN} + EM_{NL}$$

where EM_{LIN} and EM_{NL} in the mentioned example turn out to be

$$EM_{LIN} = \{2\psi_{xc}^* \Delta \langle \psi_x^* \rangle - \psi_c^* \Delta \langle \psi *_{xx} \rangle - \psi_{xxc}^* \Delta \langle \psi * \rangle\}$$

and

$$EM_{NL} = \left\{ (\Delta \langle \psi_x^* \rangle)^2 - \Delta \langle \psi^* \rangle \Delta \langle \psi_{xx}^* \rangle \right\}.$$

The EM_{LIN} term represents the linear interference effect, which involves the phase difference between the wave response and the climatological wave. The EM_{NL} term reflects the wave activity change intrinsic to the wave response itself.

References

Black, R. X. and McDaniel, B. A. (2007). Interannual Variability in the Southern Hemisphere Circulation Organized by Stratospheric Final Warming Events. *Journal of the Atmospheric Sciences*, 64(8):2968–2974.

Butler, A. H., Polvani, L. M., and Deser, C. (2014). Separating the stratospheric and tropospheric pathways of el niño–southern oscillation teleconnections. *Environmental Research Letters*, 9(2):024014.

Byrne, N. J., Shepherd, T. G., and Polichtchouk, I. (2019). Subseasonal-to-seasonal predictability of the southern hemisphere eddy-driven jet during austral spring and early summer. *Journal of Geophysical Research: Atmospheres*, 124(13):6841–6855.

Byrne, N. J., Shepherd, T. G., Woollings, T., and Plumb, R. A. (2017). Nonstationarity in Southern Hemisphere Climate Variability Associated with the Seasonal Breakdown of the Stratospheric Polar Vortex. *Journal of Climate*, 30(18):7125–7139.

Dee, D. P., Uppala, S. M., Simmons, A. J., Berrisford, P., Poli, P., Kobayashi, S., Andrae, U., Balmaseda, M. A., Balsamo, G., Bauer, P., Bechtold, P., Beljaars, A. C. M., van de Berg, L., Bidlot, J., Bormann, N., Delsol, C., Dragani, R., Fuentes, M., Geer, A. J., Haimberger, L., Healy, S. B., Hersbach, H., Hólm, E. V., Isaksen, L., Kållberg, P., Köhler, M., Matricardi, M., McNally, A. P., Monge-Sanz, B. M., Morcrette, J.-J., Park, B.-K., Peubey, C., de Rosnay, P., Tavolato, C., Thépaut, J.-N., and Vitart, F. (2011). The era-interim reanalysis: configuration and performance of the data assimilation system. *Quarterly Journal of the Royal Meteorological Society*, 137(656):553–597.

Ding, Q., Steig, E. J., Battisti, D. S., and Wallace, J. M. (2012). Influence of the Tropics on the Southern Annular Mode. *Journal of Climate*, 25(18):6330–6348.

Fletcher, C. G. and Kushner, P. J. (2011). The Role of Linear Interference in the Annular Mode Response to Tropical SST Forcing. *Journal of Climate*, 24(3):778–794.

Fogt, R. L. and Bromwich, D. H. (2006). Decadal variability of the enso teleconnection to the high-latitude south pacific governed by coupling with the southern annular mode. *Journal of Climate*, 19(6):979–997.

Fogt, R. L., Bromwich, D. H., and Hines, K. M. (2011). Understanding the sam influence on the south pacific enso teleconnection. *Climate Dynamics*, 36(7):1555–1576.

Hio, Y. and Yoden, S. (2005). Interannual Variations of the Seasonal March in the Southern Hemisphere Stratosphere for 1979–2002 and Characterization of the Unprecedented Year 2002. *Journal of the Atmospheric Sciences*, 62(3):567–580.

Hurwitz, M. M., Newman, P. A., Oman, L. D., and Molod, A. M. (2011). Response of the Antarctic Stratosphere to Two Types of El Niño Events. *Journal of the Atmospheric Sciences*, 68(4):812–822.

Ineson, S. and Scaife, A. A. (2009). The role of the stratosphere in the european climate response to el niño. *Nature Geoscience*, 2(1):32–36.

Jha, B., Kumar, A., and Hu, Z.-Z. (2016). An update on the estimate of predictability of seasonal mean atmospheric variability using north american multi-model ensemble. *Climate Dynamics*, pages 1–13.

Kidson, J. W. (1999). Principal modes of southern hemisphere low-frequency variability obtained from ncep-ncar reanalyses. *Journal of Climate*, 12(9):2808–2830.

Kuroda, Y. and Kodera, K. (1998). Interannual variability in the troposphere and stratosphere of the southern hemisphere winter. *Journal of Geophysical Research: Atmospheres*, 103(D12):13787–13799.

L'Heureux, M. L. and Thompson, D. W. J. (2006). Observed Relationships between the El Niño–Southern Oscillation and the Extratropical Zonal-Mean Circulation. *Journal of Climate*, 19(2):276–287.

Lin, P., Fu, Q., and Hartmann, D. L. (2012). Impact of Tropical SST on Stratospheric Planetary Waves in the Southern Hemisphere. *Journal of Climate*, 25(14):5030–5046.

Mo, K. C. (2000). Relationships between low-frequency variability in the southern hemisphere and sea surface temperature anomalies. *J. Climate*, 13(20):3599–3610.

Molteni, F., Stockdale, T., Alonso-Balmaseda, M., Balsamo, G., Buizza, R., Ferranti, L., Magnusson, L., Mogensen, K., Palmer, T., and Vitart, F. (2011). The new ecmwf seasonal forecast system (system 4). (656):49.

Osman, M., Vera, C. S., and Doblas-Reyes, F. J. (2016). Predictability of the tropospheric circulation in the southern hemisphere from chfp models. *Climate Dyn.*, 46(7):2423–2434.

Preisendorfer, R. W. and Barnett, T. P. (1983). Numerical Model-Reality Intercomparison Tests Using Small-Sample Statistics. *Journal of the Atmospheric Sciences*, 40(8):1884–1896.

Sardeshmukh, P. D. and Hoskins, B. J. (1988). The Generation of Global Rotational Flow by Steady Idealized Tropical Divergence. *Journal of the Atmospheric Sciences*, 45(7):1228–1251.

Seager, R., Harnik, N., Kushnir, Y., Robinson, W., and Miller, J. (2003). Mechanisms of Hemispherically Symmetric Climate Variability*. *Journal of Climate*, 16(18):2960–2978.

Seviour, W. J. M., Hardiman, S. C., Gray, L. J., Butchart, N., MacLachlan, C., and Scaife, A. A. (2014). Skillful Seasonal Prediction of the Southern Annular Mode and Antarctic Ozone. *Journal of Climate*, 27(19):7462–7474.

Shepherd, T. G., Polichtchouk, I., Hogan, R., and Simmons, A. J. (2018). Report on the stratosphere task force. Technical Report 824, European Center for Medium-Range Weather Forecasts.

Silvestri, G. and Vera, C. (2009). Nonstationary impacts of the southern annular mode on southern hemisphere climate. *J. Climate*, 22(22):6142–6148.

Silvestri, G. E. and Vera, C. S. (2003). Antarctic oscillation signal on precipitation anomalies over southeastern south america. *Geophysical Research Letters*, 30(21).

Smith, K. L., Fletcher, C. G., and Kushner, P. J. (2010). The Role of Linear Interference in the Annular Mode Response to Extratropical Surface Forcing. *Journal of Climate*, 23(22):6036–6050.

Takaya, K. and Nakamura, H. (2001). A Formulation of a Phase-Independent Wave-Activity Flux for Stationary and Migratory Quasigeostrophic Eddies on a Zonally Varying Basic Flow. *Journal of the Atmospheric Sciences*, 58(6):608–627.

Thompson, D., Baldwin, M., and Solomon, S. (2005). Stratosphere–troposphere coupling in the southern hemisphere. *Journal of The Atmospheric Sciences - J ATMOS SCI*, 62.
Thompson, D. W. J. and Wallace, J. M. (2000). Annular Modes in the Extratropical Circulation. Part I: Month-to-Month Variability. *Journal of Climate*, 13(5):1000–1016.
Vera, C., Silvestri, G., Barros, V., and Carril, A. (2004). Differences in el niño response over the southern hemisphere. *Journal of Climate*, 17(9):1741–1753.
Wigley, T. M. L. and Santer, B. D. (1990). Statistical comparison of spatial fields in model validation, perturbation, and predictability experiments. *Journal of Geophysical Research: Atmospheres*, 95(D1):851–865.
Wilson, A. B., Bromwich, D. H., and Hines, K. M. (2016). Simulating the mutual forcing of anomalous high southern latitude atmospheric circulation by el niño flavors and the southern annular mode. *Journal of Climate*, 29(6):2291 – 2309.
Zubiaurre, I. and Calvo, N. (2012). The el niño–southern oscillation (enso) modoki signal in the stratosphere. *Journal of Geophysical Research: Atmospheres*, 117(D4).

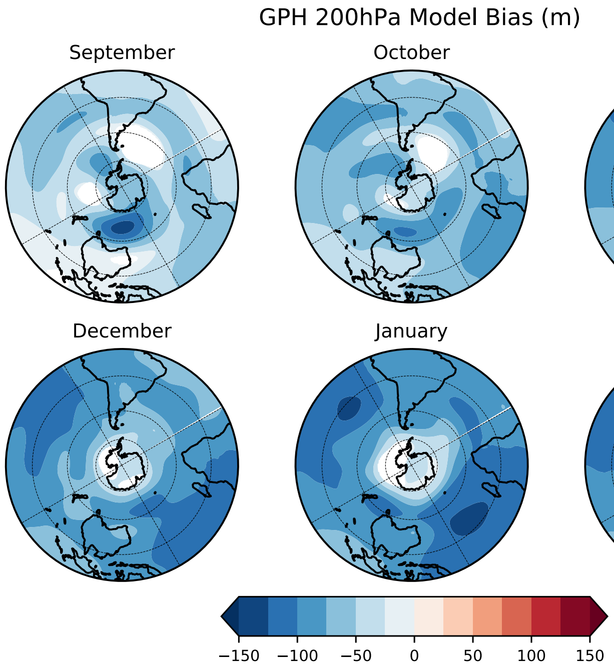

Fig. 1 Monthly mean climatological differences in Z between hindcasts and ERA-Interim (m) for (a) September, (b) October, (c) November, (d) December, (e) January, (f) February 1981-2018. The year 2002 has been excluded. Coloured regions indicate differences that are statistically different at the 5% level based on a two-sided t-test. Hindcasts are initialized on 1 August.

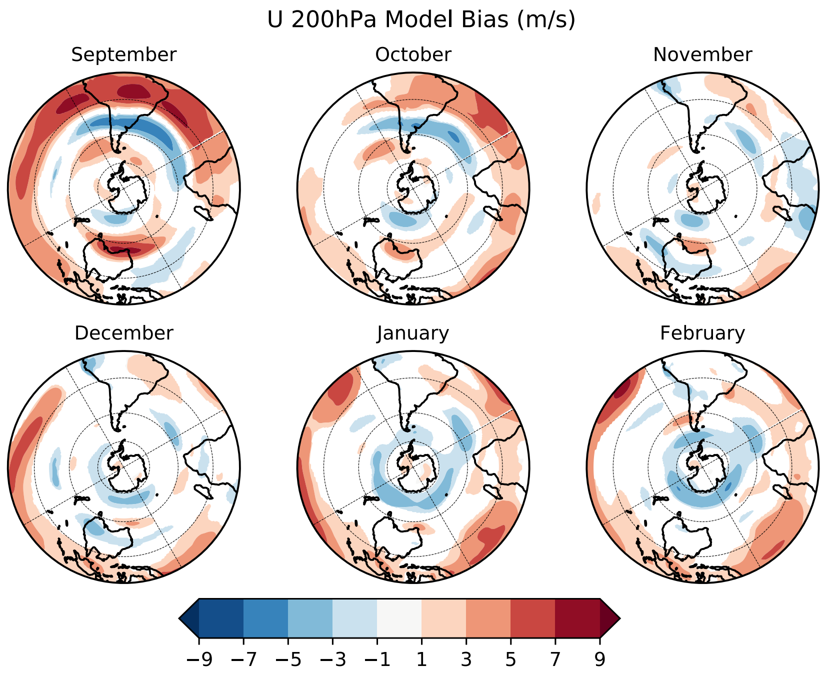

Fig. 2 Same as Figure 1 but for zonal wind u.

Table 1 Number of cases by category used in the composites based on the joint SPV-ENSO distribution shown in Figure 5.

	Strong SPV	Neutral SPV	Weak SPV	Sum
Niño	65	236	158	459
Neutral	255	452	211	918
Niña	139	230	90	459
Sum	459	918	459	1836

Table 2 Composites computed to analyze the response to ENSO and SPV.

Composite	Reference
Weak - Strong SPV cond Niño	SPV composites cond Niño
Weak - Strong SPV cond Niña	SPV composites cond Niña
Niño - Niña cond Strong SPV	ENSO composites cond Strong SPV
Niño - Niña cond Weak SPV	ENSO composites cond Weak SPV
Niño & Weak SPV	In-phase events
Niña & Strong SPV	In-phase events
Niño & Strong SPV	Out-of-phase events
Niña & Weak SPV	Out-of-phase events

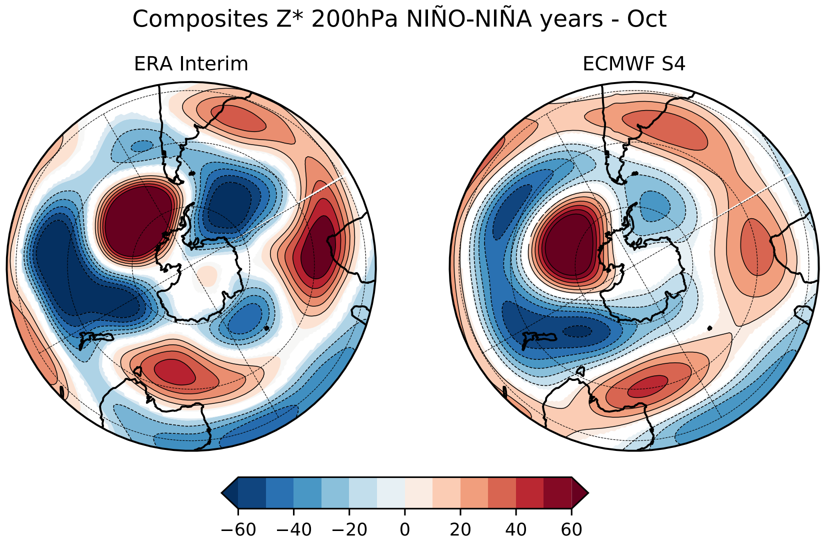

Fig. 3 Composite differences of Z^* at 200hPa between El Niño and La Niña in October for (a) ERA-Interim and (b) hindcasts. Units are in m and coloured regions are statistically different from zero at the 5% level based on a t-test.

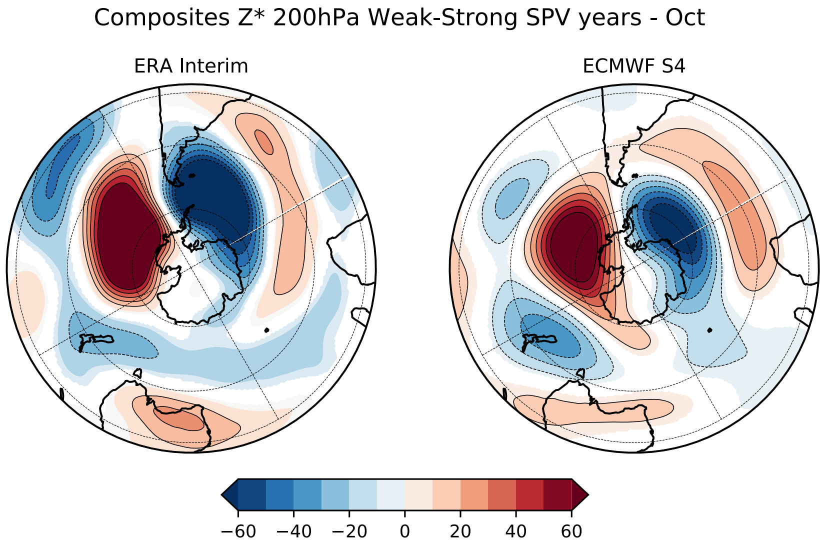

Fig. 4 Composite differences of Z^* at 200hPa between weak and strong SPV in October for (a) ERA-Interim and (b) hindcasts. Units are in m and coloured regions are statistically different from zero at the 5% level based on a t-test.

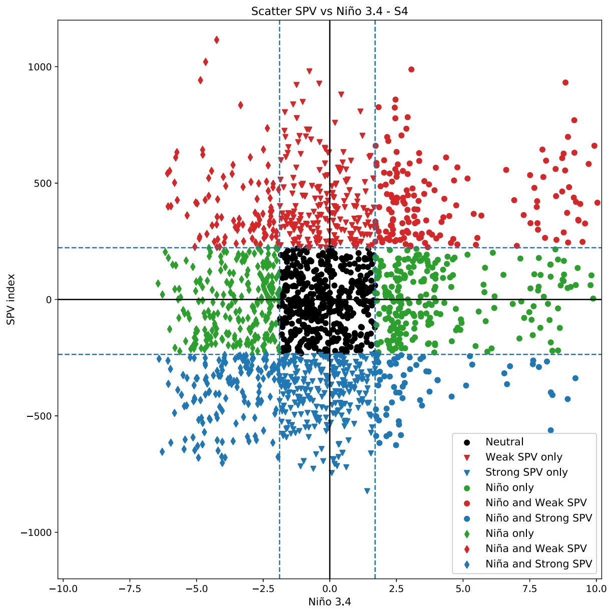

Fig. 5 Scatter plot between ENSO and SPV indices. Red (blue) symbols denote weak (strong) SPV events, which correspond to positive (negative) SPV indices. Horizontal and vertical dashed lines define the limits of each category. Green colours are used for neutral SPV events that occur simultaneously with either positive or negative ENSO events while triangles denote neutral ENSO events that occur simultaneously with either strong or weak SPV events.

Table 3 Pattern correlation between monthly composites of Z^* at 50hPa for Strong/Weak SPV and those for in phase and out of phase events. Bold (italic) denotes correlations statistically different from ± 1 at the 5% and (10%) levels based on a Pool Permutation Procedure.

	Sep	Oct	Nov	Dec	Jan	Feb
Weak-Strong SPV cond El Niño vs Weak-Strong SPV cond La Niña	0.98	0.98	0.93	0.92	0.39	0.71
El Niño-La Niña cond Weak SPV vsi El Niño-La Niña cond Strong SPV	0.90	0.78	0.94	0.67	*0.79*	0.90
El Niño-Weak SPV vs La Niña-Strong SPV	-0.95	-0.97	-0.86	-0.60	-0.65	-0.94
El Niño-Strong SPV vs La Niña-Weak SPV	-0.96	-0.94	-0.47	-0.98	-0.84	-0.74

Table 4 Same as Table 3 but for composites at 200hPa.

	Sep	Oct	Nov	Dec	Jan	Feb
Weak-Strong SPV cond El Niño vs Weak-Strong SPV cond La Niña	0.87	0.95	**0.89**	**0.67**	**0.38**	**0.47**
El Niño-La Niña cond Weak SPV vs El Niño-La Niña cond Strong SPV	0.93	0.90	**0.89**	**0.78**	*0.85*	0.85
El Niño-Weak SPV vs La Niña-Strong SPV	-0.73	-0.97	-0.97	-0.89	-0.81	-0.81
El Niño-Strong SPV vs La Niña-Weak SPV	-0.79	-0.77	-0.69	-0.53	-0.62	-0.53

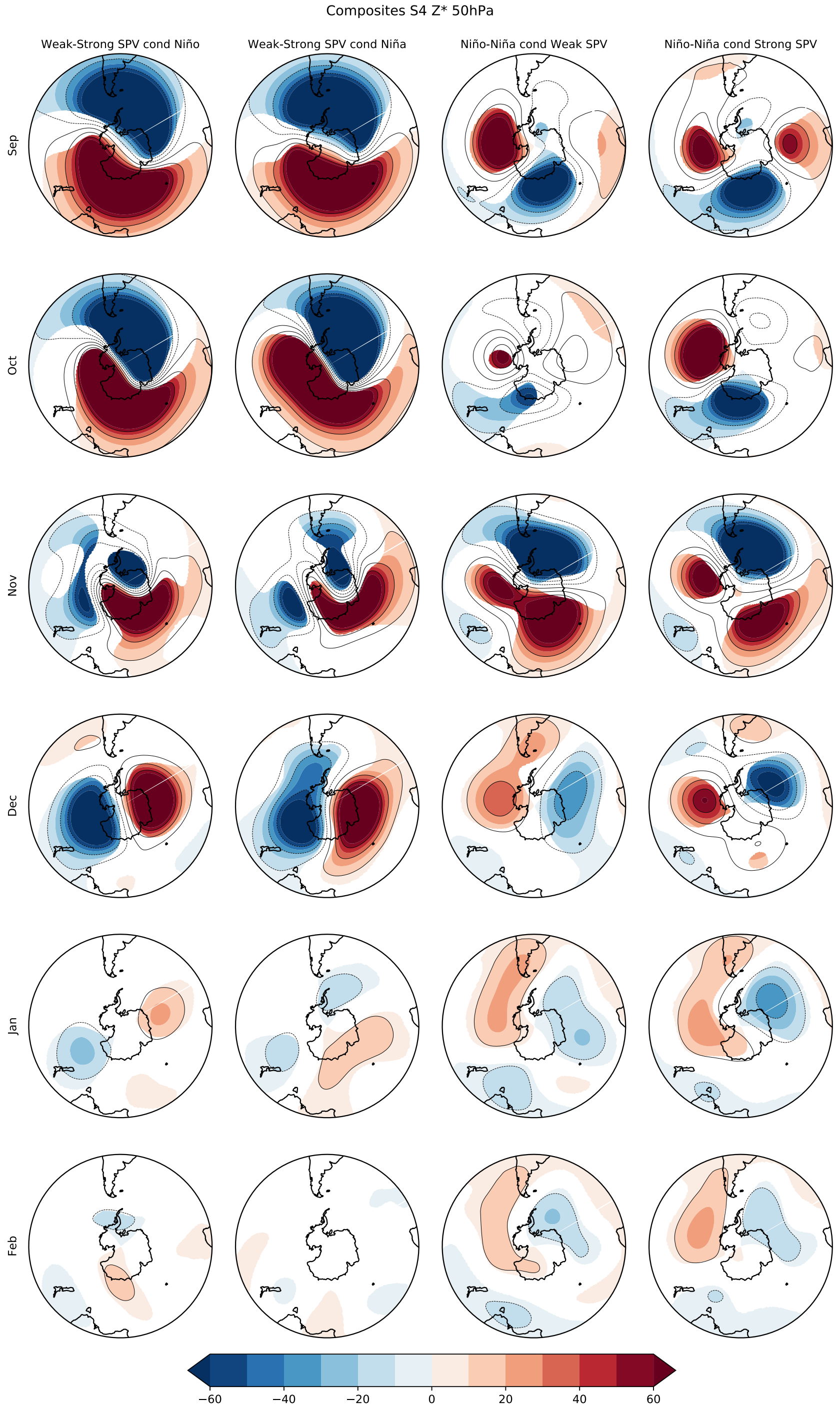

Fig. 6 Monthly mean Z^* at 50hPa composites for: Weak minus Strong SPV conditioned on El Niño events (first column); Weak minus Strong SPV conditioned on La Niña events (second column); El Niño minus La Niña conditioned on Weak SPV (third column); El Niño minus La Niña conditioned on Strong SPV (fourth column). Contour intervals are 20m. Coloured regions are statistically different from zero at the 5% level based on a t-test.

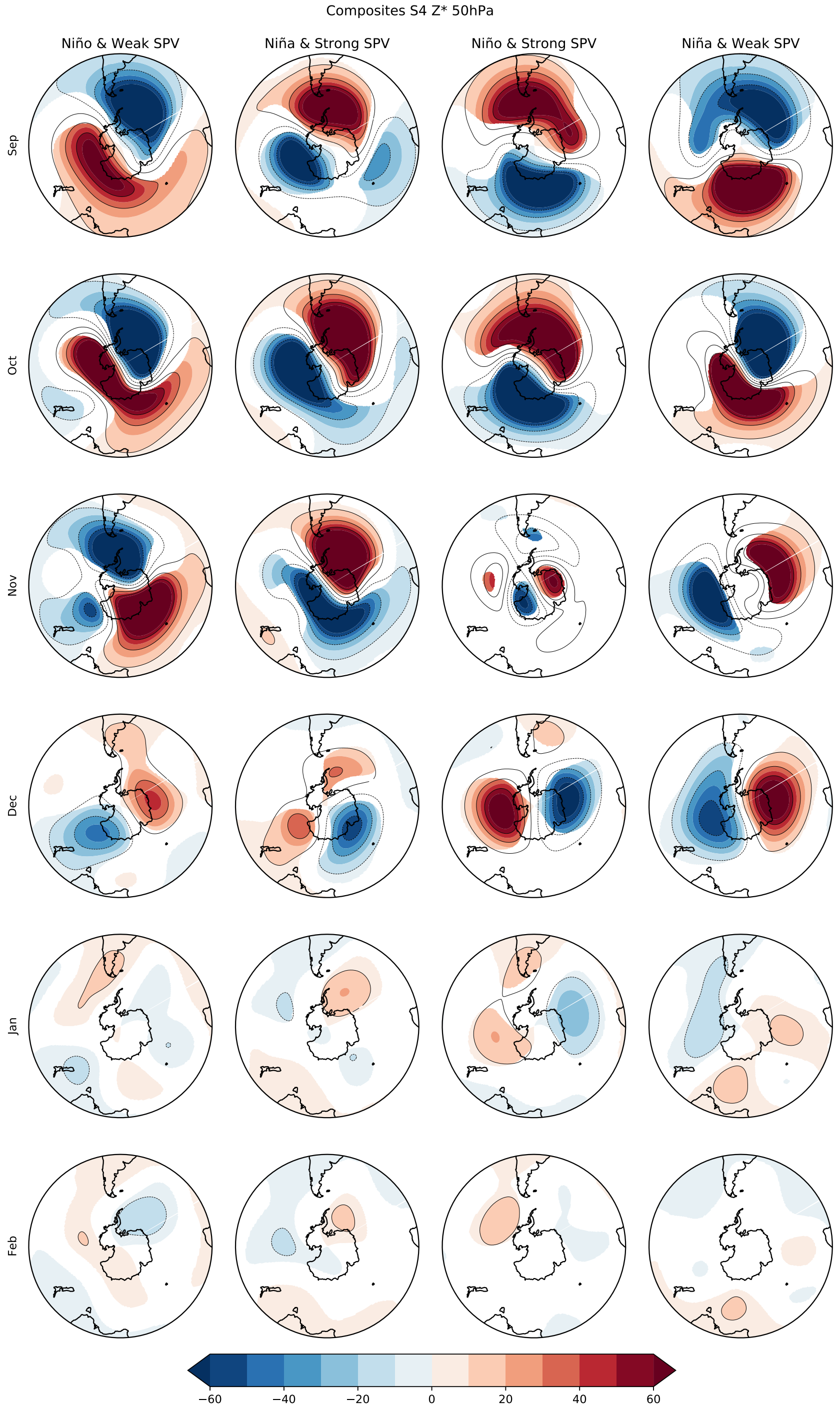

Fig. 7 Monthly mean Z^* at 50hPa anomaly composites for: El Niño-weak SPV (first column); La Niña-strong SPV (second column); El Niño-strong SPV (third column); La Niña-weak SPV (fourth column). Contour intervals are 20m. Coloured regions are statistically different from zero at the 5% level based on a t-test.

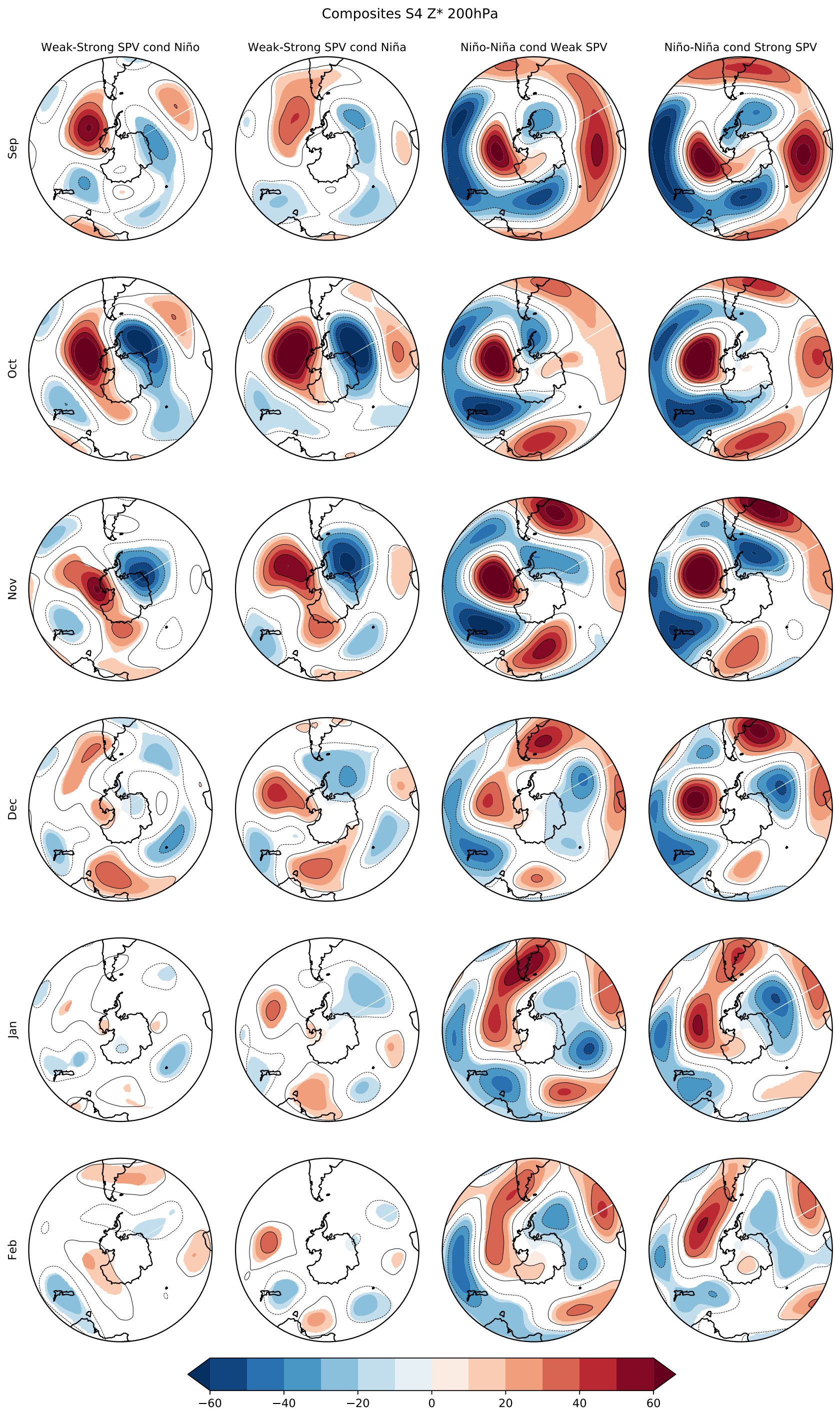

Fig. 8 Same as Fig. 6 but for Z^* differences at 200hPa.

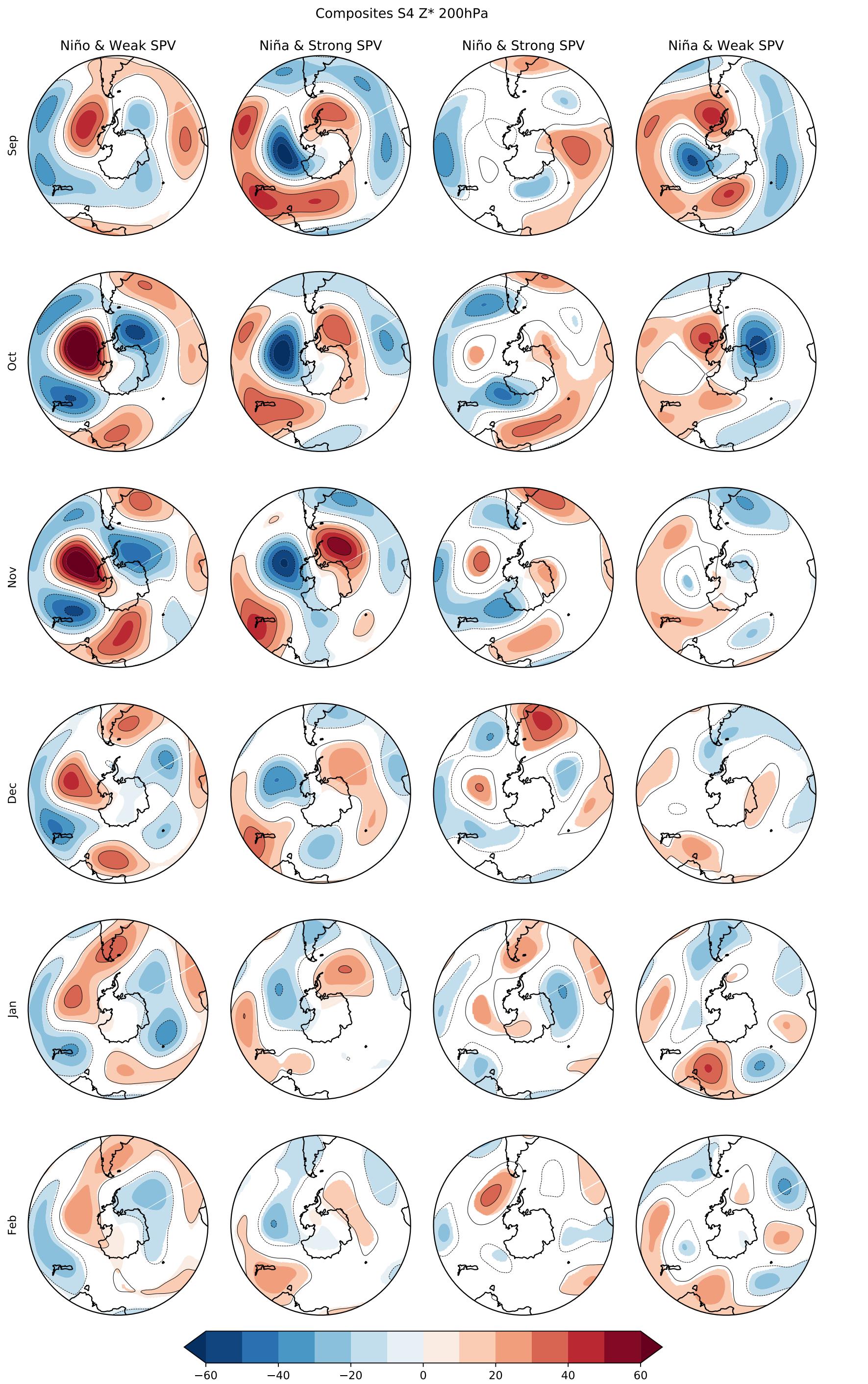

Fig. 9 Same as Fig. 7 but for Z^* differences at 200hPa.

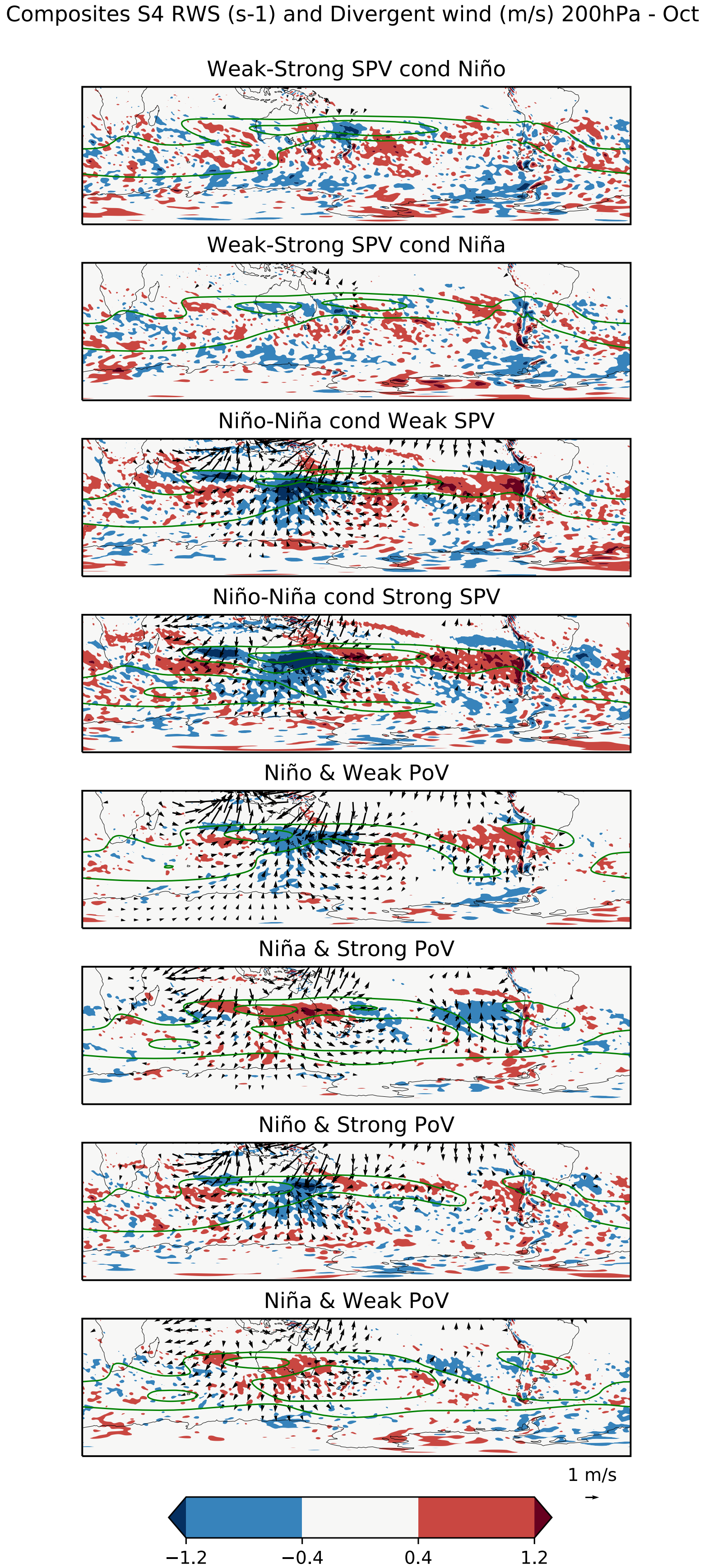

Fig. 10 Composite differences of Rossby Wave Source (shaded, units 1e-10 s^{-1}) and divergent wind (arrows, units m/s) at 200hPa for the eight categories defined in Table 1 against climatology. Zonal wind values are displayed in green contours (contour values: 30m/s and 40 m/s).

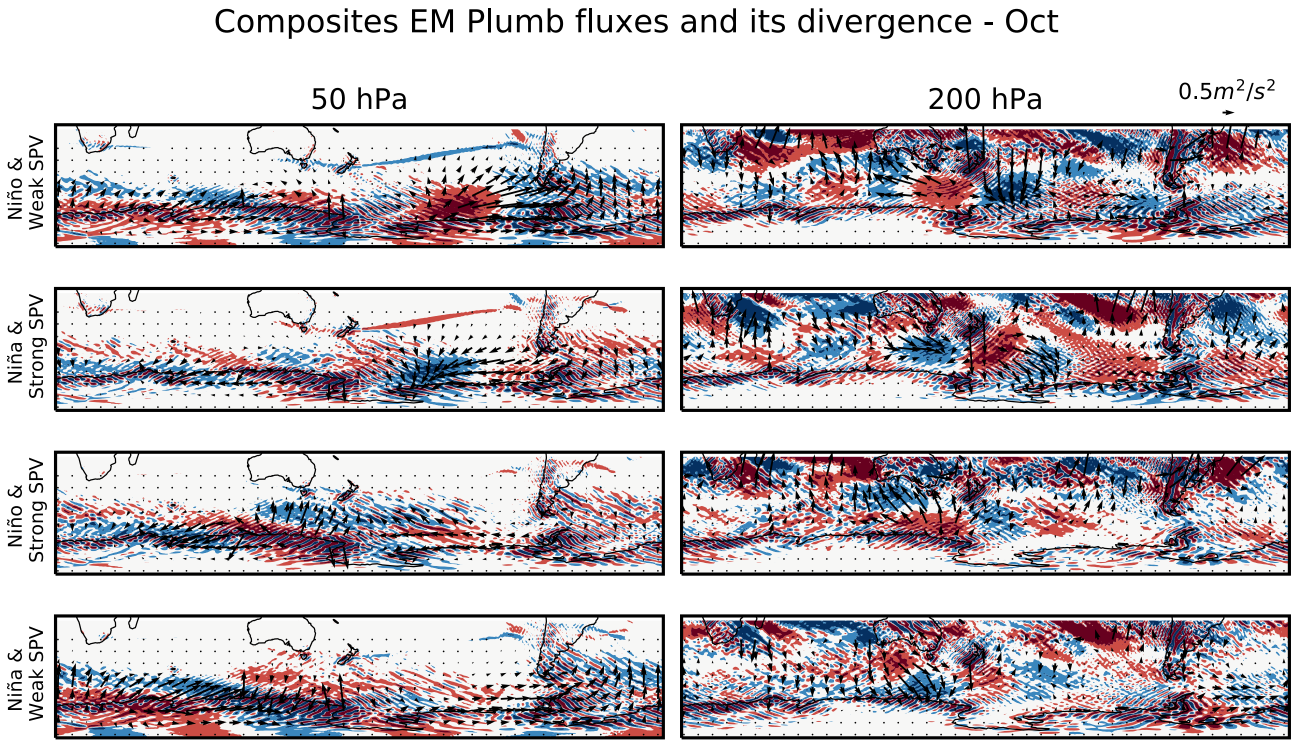

Fig. 11 Ensemble mean Wave activity Flux response (arrows) and its divergence (shaded) at 50hPa (left column) and 200hPa (right column) to in-phase and out-of-phase events. Convergence/Divergence levels are ± 0.3e-6ms^{-2} and ± 1e-6ms^{-2}.

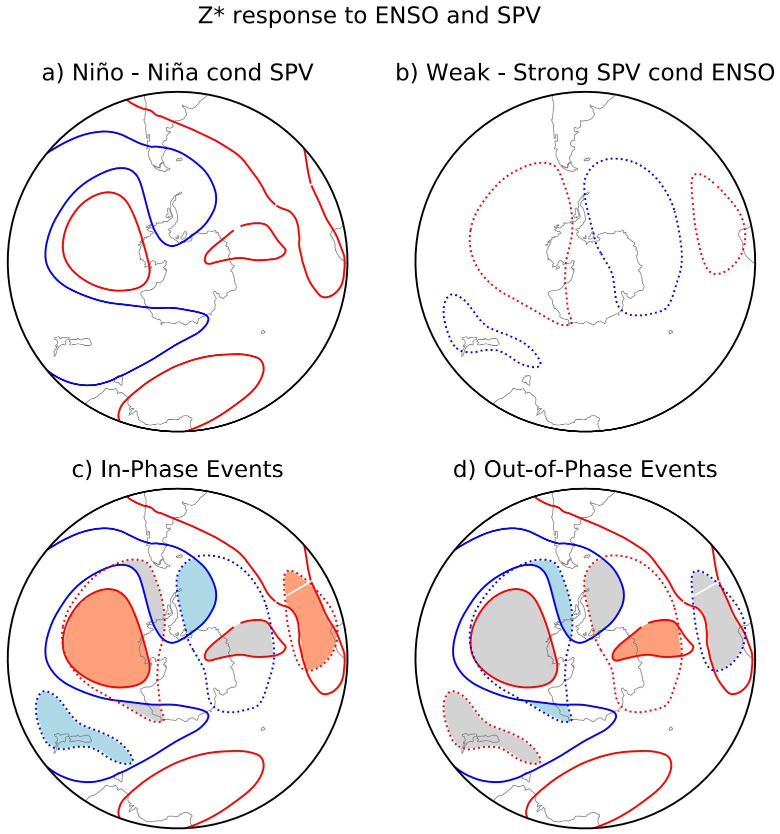

Fig. 12 Schematic showing the role of ENSO and SPV on Z* at 200hPa during springtime. a) El Niño minus La Niña composites conditioned on SPV, b) Weak minus Strong SPV conditioned on ENSO, c) In-phase events (El Niño (solid lines) and Weak SPV (dotted lines) events; composites for La Niña and Strong SPV events are similar but with opposite signs), d) Out-of-phase events (El Niño (solid lines) and Strong SPV (dotted lines) events; composites for La Niña and Weak SPV events are similar but with opposite signs). Red lines denote positive anomalies while blue lines denote negative anomalies. Red (blue) shading in c) and d) denotes regions where positive (negative) anomalies are reinforced due to the combination of ENSO and SPV, while gray shading denotes regions where anomalies partially cancel.